

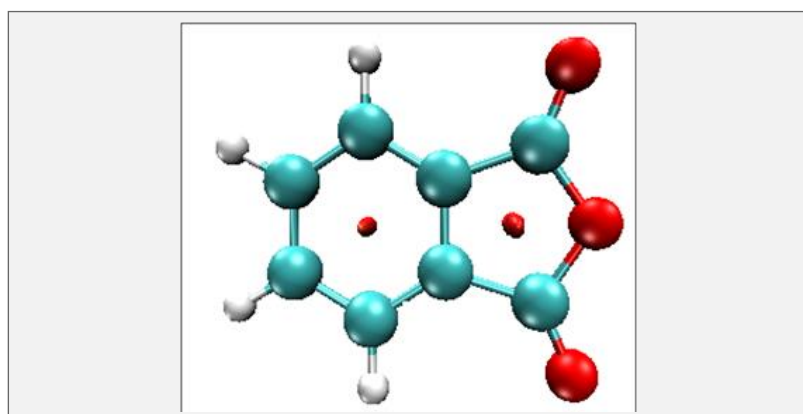
Full Paper | <http://dx.doi.org/10.17807/orbital.v15i5.17679>

Investigations on Growth, Characterization, NCI-RDG, AIM, Molecular Docking and *In-Silico* ADME Properties of 1,2-Benzene Dicarboxylic Acid Anhydride

G. Saravana Kumar* ^a, M. Jeyalaxmi ^b, N. Boukabcha ^{c,d}, K. Vijayanarasimhan ^a, and A. Chouaih ^d

Superior single crystal of 1,2-benzene dicarboxylic acid anhydride additionally called Phthalic anhydride (PAN) was developed via solution growth at low temperatures. Single crystal X-ray diffraction investigation revealed the crystal system and unit cell characteristics. The phase stability and crystalline nature were uncovered by powder X-ray diffraction analysis. FT-IR examination was done for the titular material so as to survey the various functional groups. With the use of the VEDA program's relevant resources, vibrational assignments have been made on the concept of Potential Energy Distribution (PED). Density Functional Theory (DFT) was employed to smooth out the molecular structure of PAN and was additionally utilized to consider FT-IR spectrum at molecular level. Non covalent interactions reduced density gradient (NCI-RDG) analysis has been used for the prediction of the weak interaction in the actual space in terms of the electron density along with its derivatives for PAN. Atoms in Molecules (AIM) analysis was carried for out for PAN. The docking research of the small molecule (PAN) with target protein confirmed that this is a great molecule which docks nicely with numerous targets associated with Hypoxia Inducible Factor 1- α . The absorption, distribution, metabolism, excretion (ADME) characteristics have been calculated with the assist of online server preADMET.

Graphical abstract



Keywords

ADME
Crystal
DFT
HIF1A
VEGF

Article history

Received 22 Dec 2022
Revised 25 Dec 2023
Accepted 31 Jan 2024
Available online 01 May 2024

Handling Editor: Arlan Gonçalves

1. Introduction

^a Department of Physics, Rajalakshmi Engineering College (Autonomous), Thandalam, Chennai-602105, Tamil Nadu, India. ^b Department of Physics, Prince Shri Venkateshwara Padmavathy Engineering College, Ponmar, Chennai – 600127, Tami Nadu, India. ^c Chemistry Department, Faculty of Exact Sciences and Informatic, Hassiba Benbouali University, Chlef 02000, Algeria. ^d Laboratory of Technology and Solid Properties (LTPS), Abdelhamid Ibn Badis University of Mostaganem, 27000 Mostaganem, Algeria. *Corresponding Author: E-mail: saravana2829@gmail.com

Even with the remarkable advancements in cancer diagnosis and therapy, pancreatic cancer still has an unusually high mortality rate [1]. Since it is frequently discovered in an advanced stage, the prognosis for the patient is generally very bad [2]. It is believed that intratumoral hypoxia is a crucial aspect of solid tumours and that it induces the production of Hypoxia Inducible Factor 1- α (HIF1A). Previous research has shown that HIF1A is fundamentally essential for maintaining the energy metabolism of tumour cells, angiogenesis, and growth and metastasis [3,4,5]. In the central nervous system (CNS), hypoxia has a profound impact on a variety of important signalling molecules [6]. Hypoxia prevents HIF1A's prolyl hydroxylation, which causes the transcription factor to aggregate and become functional [7]. HIF1A, or hypoxia-inducible factor-1, is a crucial transcriptional factor that allows cells to change in response to low oxygen tension [8]. HIF1A is recognised as the initial step in the antigenic process in tumour cells because to the transcriptional activation of cancer-related genes like the vascular endothelial growth factor (VEGF) gene [9]. Poorly differentiated lesions have a higher pathogenic stage than well-differentiated lesions due to the degree of HIF1A. High proliferation, increased ER and VEGF expressions, and increased HIF1A levels all go hand in hand [10]. Therefore, the high level of HIF1A has the potential to be linked to more large tumours.

1,2-benzenedicarboxylic acid anhydride otherwise called phthalic anhydride (PAN) is an organic chemical with the formula $C_8H_4O_3$. It is a white crystalline material with a molar mass of 148.11 g/mol that is used in the synthesis of pigments, dyes, pharmaceuticals, food additives, plasticizers, and other essential industrial chemicals [11]. As theoretical investigations and forecast shows a great deal of information, useful and reliable data before proceeding towards clinical level trials. Our aim was to explore the pharmacological activity of PAN at molecular scale. Although there are various reports on titular material to explore its potential application in several fields, we attempted to explore some interesting facts of PAN in the field of pharmacology. Recent studies [12,13], demonstrated the pharmacological activity of PAN and PAN based compounds as a potential candidate for biological applications. This provoked us to explore further the pharmacological activity of PAN. The initial screening of PAN revealed its ability as a potential hypoxia inducible factor 1- α (HIF1A) inhibitors. The present investigation hurl light on the crystal growth, structural analysis, spectral analysis, DFT, NCI-RDG and AIM analysis. A special emphasis on Molecular docking and ADME properties of PAN are reported.

2. Material and Methods

2.1 Crystal Growth

For crystallization, Merck's commercially available phthalic anhydride (AR grade - 98%) was used. The slow evaporation approach was used to grow the PAN single crystals. For the development of a single crystal of PAN, ethanol was used as the solvent. In order to establish homogeneity, the saturated ethanolic solution of titular material was stirred for 8 hours using an immersible magnetic pellet that was placed on a magnetic stirrer. Using a Whatmann filter paper, the fluid was filtered. To reduce the rate of evaporation, aluminum foil was placed on top of the solution. After 18 days, the PAN single crystal of high purity was obtained using a slow evaporation method. The image of a single PAN crystal as it has developed is depicted in Fig. 1.



Fig. 1. Photograph of as grown crystal of PAN.

2.2 Computational Details

The Gaussian 09W [14] package's 6-311++G(d,p) premise set functions of the Density Functional Theory (DFT) and gradient geometry optimization at B3LYP levels are used to do the comprehensive estimation of PAN. Using DFT [15, 16], Becke's three-parameter hybrid functional [17], the Lee-Yang-Parr correlation [18] functional (B3LYP) method, and the Gauss view programme [19], all of the mathematical borders were smoothed out using the 6-311++G(d,p) basis set. For subsequent computations, including DFT, the CCDC deposition number 1232675 and the Cambridge Structural Database (CSD) were utilised to produce the Crystallographic Information File (CIF) [20]. The AutoDockTools (ADT) v1.5.4 and AutoDock v4.2 programme (AutoDock, Auto grid, Autotors, Copyright-1991-2000) of the Scripps Research Institute (<http://www.scripps.edu>) were used as the bioinformatics tools for this experiment. The absorption, distribution, metabolism, and excretion (ADME) properties were computed using Pre-ADMET, an internet server (<http://preadmet.bmdrc.org>).

3. Results and Discussion

3.1 Single crystal X-ray diffraction analysis

The single crystal X-ray diffraction analysis has established the unit cell properties and crystal system of phthalic anhydride. For the titular material, the following lattice characteristics and crystal system were noted: volume $V = 659.96 (3) \text{ \AA}^3$, orthorhombic crystal system, $a = 7.889 (2) \text{ \AA}$, $b = 14.155 (2) \text{ \AA}$, $c = 5.910 (7) \text{ \AA}$. The phthalic anhydride crystal generated in this inquiry utilising ethanol as the solvent was determined to have agreeable lattice parameters and crystal system as that of the reported data Table 1 [20], according to the single crystal X-ray diffraction examination. So, as is asserted, the titular substance crystallises as phthalic anhydride.

3.2 Analysis of powder X-ray diffraction

To evaluate the sample purity, stable phase, and crystallinity of the powdered sample of single crystals of phthalic anhydride, powder X-ray diffraction examination was conducted. It is common knowledge that the pharmacologically active substances are only presented as commercial drugs after undergoing rigorous testing. Additionally, it is clear that these medicines, which have been approved following a number of clinical trials, are taken in virtually powdered crystalline form. As a result, we made an effort to examine the specifics of the titular material's powdered sample. We tried to compare the experimental powder X-ray diffractogram with the powder X-ray pattern simulated from the Crystallographic Information File (CIF) using Mercury software, which is available from

Cambridge Crystallographic Data Centre (CCDC), in order to have a clear understanding about the stable phase of the titular material. Fig. 2 shows the phthalic anhydride powder X-ray diffraction pattern in comparison. The consistency between the computed and experimental powder X-ray diffraction patterns is shown from Fig. 2. In terms of a high intense peak at 27.3° at the 2θ axis indexed with (201) plane, the experimental powder X-ray diffraction results are in good agreement with the model powder X-ray pattern. The study shows that the substance only contains a stable form of phthalic anhydride; no other polymorphs or unstable forms were seen during crystallisation. Furthermore, the obvious crystalline nature of the title is confirmed by the strong Bragg peaks at specified 2θ and the sharp intensities in the powder X-ray diffractogram.

Table 1. Crystal data and refinement parameters for 1,2 - Benzene Dicarboxylic Acid Anhydride.

Code CCDC	1232675 [20]
Chemical formula	C ₈ H ₄ O ₃
Molecular weight	148.11 g.mol ⁻¹
Temperature	295 K
Radiation wavelength	0.71073 Å
Crystal System	Orthorhombic
Space group	P na2 ₁
a	7.859(5) Å
b	14.173(5) Å
c	5.911(3) Å
α	90°
β	90°
γ	90°
V	658.4 Å ³
Z	4
Density	1.494 g.cm ⁻³
M	0.117 mm ⁻¹
F(000)	304.0
θ range for data correction	10° – 70°
Reflections	-4 ≤ h ≤ 4, -5 ≤ k ≤ 5, -2 ≤ l ≤ 2
R[F ² > 2s(F ²)], wR(F ²), S	0.0370, 0.0370, 1.01

3.3 Analysis of molecular geometry

To model ideal geometry and ascertain many elements of molecule structure, stability, and reactivity, computational methods are one of the informative and practical tools [21]. The entire DFT analysis is built around the improved molecular geometry. In order to refine the titular material's molecular geometry for further research on molecular structure analysis and FT-IR analysis at B3LYP/6-311++G(d,p) level in gas phase, the CIF [20] was utilised as the input. The optimised molecular geometry was found to have no negative harmonic vibrational frequencies, which led to the declaration that the molecular structure was real and stable. Fig. 3 depicts the PAN molecular structure as it has been optimized in line with experimental structure. A superposition between the experimental and theoretical structures is presented in Fig. 4. Foresman and Frisch state that the calculation of geometric parameters such as bond length, bond angle, and torsion angle is successful if the deviation of the bond length between the calculated and experimental value is only about 0.01-0.02 Å and the deviation of the bond angle and torsion angle is about 1-2° [22,23]. Table 2 is a list of the experimental and the most stable optimised geometrical parameters acquired by DFT of PAN. The biggest difference between practical and theoretical results in the estimated molecular geometry for the PAN crystal occurs in the bond length C5-C6, which is around 0.0165. In terms of bond length O2-C8, the smallest difference is 0.0004. The largest deviation in the bond angle O3-C8-O2 is around 1.74°, whereas the minimum deviation in

the bond angle C8-C2-C1 is approximately 0.04°. The largest deviation in the torsion angle O2-C8-C2-C1 is determined to be 3.2444°, and the least deviation is found at C4-C5-C6-C1 and is 0.0434°. The average difference in the length of the C-C bond between experimental and theoretical values is 0.0073. Similar to this, there is a 0.04833° average difference between the experimental and theoretical C-C-C bond angles. The significant angle variations between the observed and theoretical bond angles for the molecules C4-C5-C6, O1-C7-O3, O3-C8-O2, and O2-C8-C2 are 1.49, 1.58, 1.74, and 1.08°, respectively. The experimental data from the previous report [20] is related to the solid-state structure, whereas the calculated data is obtained in the gas phase, as can be seen in Table 2. This is to be expected since the calculated geometrical parameters are slightly longer and shorter than experimental values.

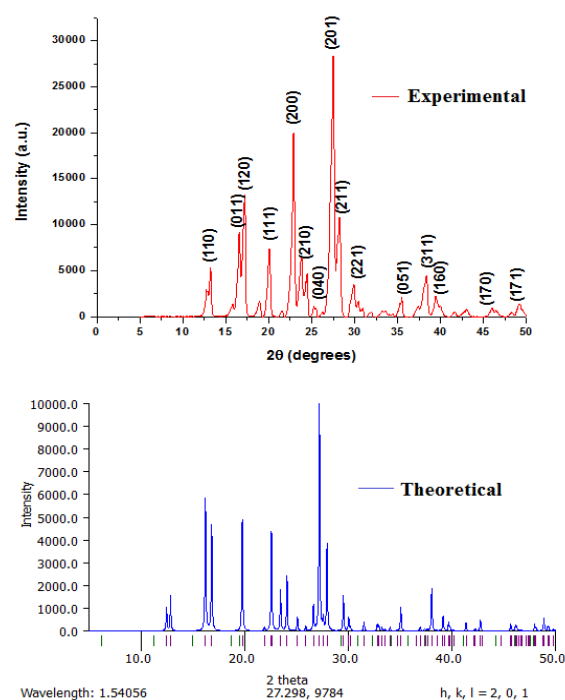


Fig. 2. Comparative powder X-ray diffraction pattern of PAN.

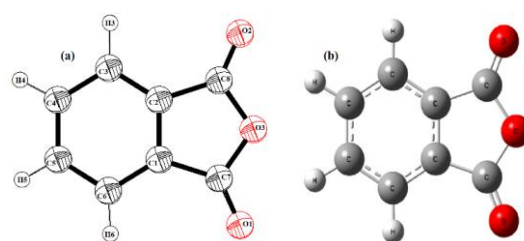


Fig. 3. (a) Experimental structure and (b) optimized structure of PAN.

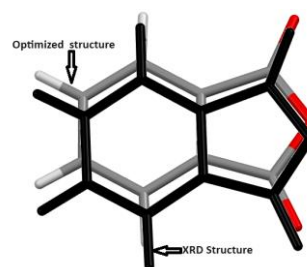


Fig. 4. Superposition of experimental and theoretical structures.

Table 2. Experimental and optimized bond lengths of PAN.

Bond length	XRD(Å)	DFT(Å)	Bond length	XRD(Å)	DFT(Å)
C1-C2	1.38	1.39	O1-C7	1.19	1.19
C2-C3	1.38	1.38	C7-O3	1.39	1.39
C3-C4	1.41	1.39	O2-C8	1.19	1.19
C4-C5	1.38	1.40	C1-C7	1.46	1.48
C5-C6	1.38	1.39	C2-C8	1.47	1.48
C1-C6	1.39	1.39			
Bond Angle	XRD(°)	DFT(°)	Bond Angle	XRD(°)	DFT(°)
C1-C2-C3	122.4	121.7	O1-C7-O3	120.6	122.2
C2-C3-C4	116.5	117.1	C7-O3-C8	109.4	110.3
C3-C4-C5	120.6	121.2	O3-C8-O2	120.4	122.2
C4-C5-C6	122.7	121.2	O2-C8-C2	131.9	130.8
C6-C1-C2	121.2	121.7	C8-C2-C1	107.4	107.8
C1-C7-O1	131.8	130.8	C8-C2-C3	130.2	130.5
Dihedral Angle	XRD(°)	DFT(°)	Dihedral Angle	XRD(°)	DFT(°)
C1-C2-C3-C4	-0.71	0	O1-C7-O3-C8	-179.5	180
C2-C3-C4-C5	1.32	0.1	C7-O3-C8-O2	177.3	179.9
C3-C4-C5-C6	-0.97	-0.1	C7-C1-C2-C8	-2.4	0.1
C4-C5-C6-C1	-0.04	0.1	O2-C8-C2-C1	-176.7	-179.9
C6-C1-C2-C3	-0.28	-0.1	C8-C2-C1-C6	179.1	-179.9
C1-C7-O3-C8	0.98	-0.1	C8-C2-C3-C4	-179.8	179.9

3.4 Analysis of vibration

One useful tool for assessing the various functional groups and their vibrational modes is vibrational analysis. To determine the chemical bonding and to learn more about the molecular structure of the substance, the Fourier transform infrared (FT-IR) spectral analysis is used. Additionally, there is a potential that an ingredient will include contaminants in very small amounts when it is used in pharmaceutical applications. In order to evaluate the modes of vibration, different functional properties, and potential contaminants in PAN, we used the FT-IR technique. Fig. 5 compares the observed FT-IR spectra of PAN with the computed IR spectrum.

C-H Vibrations

For asymmetric stretching modes of vibration, the C-H stretching vibrations of heteroaromatic and aromatic compounds occur in the range 3100–2900 cm^{-1} . The asymmetric C-H stretching vibrations of the PAN were attributed to the wavenumbers computed by B3LYP/6-311++G(d,p) discovered at 3177 cm^{-1} with PED 92%, as was expected. The C-H asymmetric stretching vibrations band is identified as the FT-IR signal at 3174 cm^{-1} .

C=O and C=C Vibrations

The main bands in the 2000–1500 cm^{-1} range are caused by the stretching of the C=C and C=O bonds. One of the simplest absorptions to spot in an infrared spectrum is carbonyl stretching. Depending on the nature of C=O bond, it usually occupies the range between 1830 and 1650 cm^{-1} and is the strongest band in the spectrum [24]. The FT-IR bands are seen at 1850 and 1899 cm^{-1} in the current investigation, respectively. The experimental value for the corresponding mode of C=O vibrations with PED 90% and 82%, respectively, and the predicted value for the C=O stretching vibration

recorded at 1841 and 1898 cm^{-1} are in great agreement. The wavenumber identified as the C=C stretching vibrations of the PAN compound at 1643 and 1382 cm^{-1} in the FT-IR spectrum is strong in intensity and is compatible with the predicted value at 1642 and 1384 cm^{-1} with PED 74% and 58%, respectively. Table 3 provides a thorough explanation of normal modes based on PED. Additionally, the FT-IR spectrum of the shows unequivocally that PAN solely consists of vibrational modes caused by Carbon, Hydrogen, and Oxygen. Furthermore, it is asserted that the titular material has no evidence of contaminants due to the similarity between the experimental and computed IR spectra. Before moving forward with the experimental and practical applications, it is obvious that the computing of a material's characteristics provides numerous crucial pieces of information from the agreement of the computed IR spectrum with the experimental one.

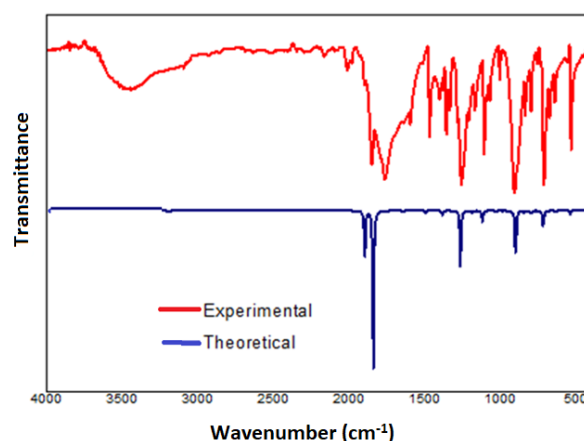
**Fig. 5.** Comparative IR spectra of PAN.

Table 3. Experimental and calculated vibrational frequencies and assignments with PED of PAN.

IR Freq. Exp.	IR Freq. cal.	Red. Masses	Force constant	IR Intensity	Assignments with PED>10%
-	124	5.1666	0.0469	0	τ OCCC(51) + τ COCC(15)
-	156	10.9727	0.1581	3.3793	τ OCCC(14) + τ COCC(47) + α OCOC(20)
-	186	7.33	0.151	0.0907	τ OCCC(11) + τ COCC(17) + α CCCC(59)
-	250	6.8531	0.2537	1.5469	β OCO(10) + β CCC(45)
-	354	11.6803	0.8668	8.1799	γ CC(13) + β COC(15) + β OCO(47)
-	416	3.0815	0.3143	0.7475	τ HCCC(11) + τ HCCC(11) + τ CCCC(59) + α CCCC(11)
-	439	5.0155	0.5708	0.0001	τ CCCC(80)
534	539	9.428	1.6182	2.5559	γ OC(17) + β CCC(29)
-	539	7.6157	1.3081	13.8096	γ CC(14) + β OCC(15)
640	637	14.076	3.3745	5.0271	γ OC(10) + β COC(51) + β OCC(15)
-	662	4.5257	1.1707	0	τ CCCC(73)
-	686	8.5453	2.3716	5.1119	β OCO(61)
715	718	2.8173	0.8568	91.7829	τ COCC(10) + α OCOC(54)
742	746	6.3593	2.0883	0.2124	γ CC(47) + β OCC(10)
-	765	8.4681	2.9267	0.0001	τ OCCC(13) + α OCOC(70)
800	800	1.7345	0.6552	14.5223	τ HCCC(49) + α OCOC(20)
840	845	7.6075	3.2066	8.4011	β CCC(39) + β OCO(33)
-	900	13.2811	6.3447	263.5724	γ OC(34) + γ OC(53)
906	905	1.3051	0.6309	0	τ HCCC(32) + τ HCCC(53)
-	987	1.3913	0.7999	1.0449	τ HCCC(60) + τ HCCC(31)
1010	1014	1.3161	0.7983	0	τ HCCC(27) + τ HCCC(32) + τ CCCC(13)
-	1029	2.3322	1.4576	5.1185	β HCC(24) + β CCC(17) + β CCC(24)
-	1104	2.5001	1.7966	0.4732	β CCC(39)
-	1121	3.9002	2.8908	55.9769	γ CC(11) + γ OC(24) + β OCO(20)
-	1186	1.1848	0.9833	11.1012	γ CC(11) + β HCC(60)
-	1189	2.1218	1.7687	0.9855	γ CC(24) + β CCC(12)
-	1266	5.8628	5.5363	261.2499	γ CC(34) + β COC(12)
-	1307	1.5567	1.5668	0.0987	β HCC(35) + β HCC(24)
1382	1384	5.9825	6.7540	22.2632	γ CC(58)
-	1497	2.5198	3.3292	0.0602	γ CC(14) + β HCC(50) + β CCC(12)
-	1497	2.4103	3.1861	9.1013	γ CC(25) + β HCC(22) + β HCC(28)
1643	1642	6.6815	10.6213	9.2060	γ CC(74)
-	1647	7.4666	11.9396	0.2028	γ CC(36) + β CCC(28)
1850	1841	13.1778	26.3319	703.7358	γ OC(90)
1899	1898	13.0769	27.7766	234.1838	γ OC(82)
3174	3177	1.0875	6.4693	1.3179	γ CH(92)
-	3190	1.091	6.5416	3.9326	γ CH(100)
-	3202	1.0942	6.6107	1.0018	γ CH(91)
-	3205	1.0966	6.6372	4.6164	γ CH(98)

γ -Stretching, β -Bending, τ -Torsion, α -Out of plane

3.5 Density gradient (NCI-RDG) analysis

Non covalent interactins reduced density gradient (NCI-RDG) analysis has been used for the prediction of the weak interaction in the actual space in terms of the electron density

along with its derivatives, which was proposed by Johnson et al. [25]. Its first derivative is expressed in the following way:

$$\text{RDG}(r) = \frac{1}{2(3\pi^2)^{\frac{1}{3}}} \frac{|\nabla\rho(r)|}{\rho(r)^{\frac{4}{3}}} \quad (1)$$

Molecular interactions are involved in the structure stability of a given material. Such interactions, act to weak intramolecular intermolecular interactions that in turn are able to be detected by reduced density gradient (RDG) analysis, this analysis relies on the analysis of non-covalent interactions (NCI) that exist in the system [26]. The NCI-RDG analysis is plotted in Fig. 6. Fig. 6 shows that the interaction is localized across an RDG isosurface that envelops their own area. Fig. 7 illustrate the gradient isosurfaces of the PAN crystal compound. Red colors indicate repulsive interactions (steric effect). The strongest steric repulsive influences of the substance have been seen in the center of the aromatic ring and furanic ring related to the π - π clustering interactions [25]. It can be seen that the steric repulsive effect is slightly large in the furan ring due to the presence of the electronegative oxygen atom. Both of steric effects might be relevant for the stability of the molecular system of the title compound.

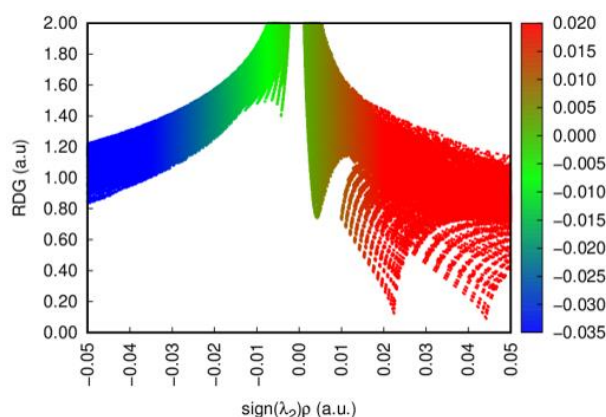


Fig. 6. The scatter diagram of PAN molecule.

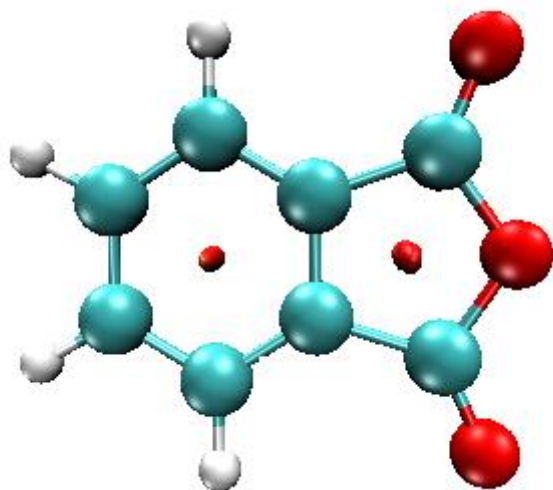


Fig. 7. The gradient isosurfaces of PAN compound.

3.6 AIM calculations: Geometrical and topological parameters

The topological analysis approach is being applied to further analyze the weakness of interactions between several substances. Atoms in Molecules (AIM) theory is often explored for identifying interaction types in a multitude of different molecular structures and for assessing the electron density at critical bond points (RCPs) [27]. The quantum theory of atoms in molecules (QTAIM) has been widely implemented as a means to classify and comprehend chemical quantum interactions such as electron density ρ . QTAIM theory effectively depicts the pattern of interactions and its conception without limit. The benefits of the AIM

theory is that it provides modification in the distribution of the electron density due to the binding formation. The geometrical and topological parameters are important elements in order to determine the strength of the hydrogen bond, bond critical points (BCPs) and ring critical points (RCPs). In our case we have ring critical points (RCPs) in the PAN compound. Those properties could be observed by means of topological parameters among the compound structures like electron density Laplacian $\nabla^2\rho(r)$, electron density $\rho(r)$, potential energy density $V(r)$, Lagrangian kinetic energy $G(r)$, kinetic Hamiltonian energy $H(r) = G(r) + V(r)$ bond energy and $E_{int} = V(r)/2$. All of these topological parameters are reported in atomic units. the optimized geometrical structure has been adopted in order to establish the critical points of the intramolecular ring (RCPs) in our crystal structure. The computational results were analyzed with the Multiwfn package [28]. The resulting molecular plot displaying the critical points in the ring of compound PAN is illustrated in Fig. 8(a). The molecular pattern of compound PAN in the RCPs molecular interactions seen by using the Multiwfn software are plotted in Fig. 8(b) and the ring points interaction topological parameters 24 and 26 for the molecule PAN are listed in Table 4. Usually, elevated $\rho(r)$ electron density readings and its laplacian $\nabla^2\rho(r)$ denote the strong interactions [25]. In the PAN molecule compound, the electron density (ρ RCP) value is 0.02232 for RCP24 and 0.04406 atomic unit for RCP26. The high RCP26 value of the electron density (RCP26) is due to the presence of an oxygen atom in the furan ring. The values of Laplacian is 0.16255 for RCP24 and 0.30662 atomic unit for RCP26. Also, the hamiltonian kinetic energy $K(r)$ of RCP26 point is higher (-0.00721 au) than the resulting value of the point RCP24 (-0.00721 au). The elevated values of RCP26 compared to RCP24 parameters presented in table 4 are caused by the electronegative oxygen atom presence in the furan ring.

3.7 Molecular docking analysis

In the realm of molecular modelling, a method called docking makes predictions about the preferred orientation of one molecule to another when they are joined to form a stable complex. Instead of using the resources in experimental labs, this offers a path and fundamental concepts for the synthesis of materials. By offering predictions of the ligand's bound shape and a plan for ranking the protein-ligand interaction energetically, molecular docking methods are particularly helpful in describing the protein-ligand interaction. To find the optimal *insilico* conformation, automated molecular docking was done with the synthesized material. Prior to docking, ligands were optimised in Gaussian 09 W [14] software using the DFT/B3LYP/6-311++G(d,p) basis set. Online programmes called PASS (Prediction of Activity Spectra) [29] forecasts many kinds of activities. Protein Data Bank (PDB), (<http://www.pdb.org>), retrieved from PASS analysis of PAN predicts actions towards the factor inhibiting HIF-1 alpha in combination with HIF-1 alpha fragment peptide (PDB ID: 1H2K). The Q-site Finder is used to look for the likely binding sites of preferred target receptors in order to identify the ligand-binding site. Protein active and binding sites are frequently linked to structural pockets and cavities. Kollman and Gasteiger charges have been added in total, totalling -6.957 and -14.0268, respectively. There are a total of 8 aromatic carbons and 4 nonpolar hydrogens in the titular material. The search was carried out using the Lamarckian Genetic Algorithm, and populations of 150 people were produced over a period of 10 generations with a mutation rate of 0.02. Following the saving of each compound in PDBQT

format, AutoDock was used to dock the compounds. The mimic structure with the lowest energy among the 10 docking options is thought to be the best one. The value of interaction between ligand and receptor was -4.45 kcal/mol. It was discovered that the hydrogen bonds between two N-H of His313A and one carbonyl oxygen atom of the five-membered ring of PAN were, respectively, 2.8 and 2.7 Å. The Asp222A N-H and one of the carbonyl oxygen atoms in the five-membered PAN ring form a 2.8 Å hydrogen connection. In Fig. 9, the same is displayed as a pose view diagram of PAN. The carbonyl oxygen atoms of the five-membered ring of PAN are more interactive with the targets.

3.8 Pre-ADME and pharmacokinetic of PAN

The Lipinski's Rule is met by the PAN molecule (Rule of Five). A substance must possess the perfect ADMET qualities in order for clinical tests to identify it as a substance. The only drug that can typically traverse cell membranes and interact with a pharmacological target is the unbound drug. As a result, a drug's plasma protein binding level affects not only how it acts but also how it is disposed of and how effective it is. Chemicals are strongly bound when the value is greater than 90%; otherwise, they are weakly bound. 52.795% is shown by the PAN. The Human Intestinal Absorption (HIA) test typically shows good, moderate, and poor absorption in the ranges of 70–100, 20–70, and 0–20%. PAN revealed intestinal absorption of 97.262%, which is considered "good" absorption in human intestine. PAN's cell permeability was observed to be 6.1217×10^{-6} cm/sec. Maden Darby Canine Kidney (MDCK) cell permeability is divided into three categories: low (less than 2.5×10^{-6} cm/sec), moderate (between 2.5 and 50.0×10^{-6} cm/sec), and high (beyond 50.0×10^{-6} cm/sec). In in-vitro MDCK cells, PAN displayed medium permeability at 6.1217×10^{-6} cm/sec. The Blood Brain Barrier (BBB) is a direct index of a drug's ability to set foot in the central nervous system (CNS). Low, moderate, and high (below 0.1 b/b, 0.1 to 2.0 b/b, and above 2.0 b/b) are the classifications. PAN in BBB is 1.22044, which indicates a moderate value for penetration. In the pharmaceutical, cosmetic, and agrochemical industries, it is crucial to anticipate the skin permeability rate for the transdermal administration of drugs and for the risk evaluation of all substances that come into contact with the skin either accidentally or on purpose. Skin permeability for PAN is -2.5519 cm/hour.

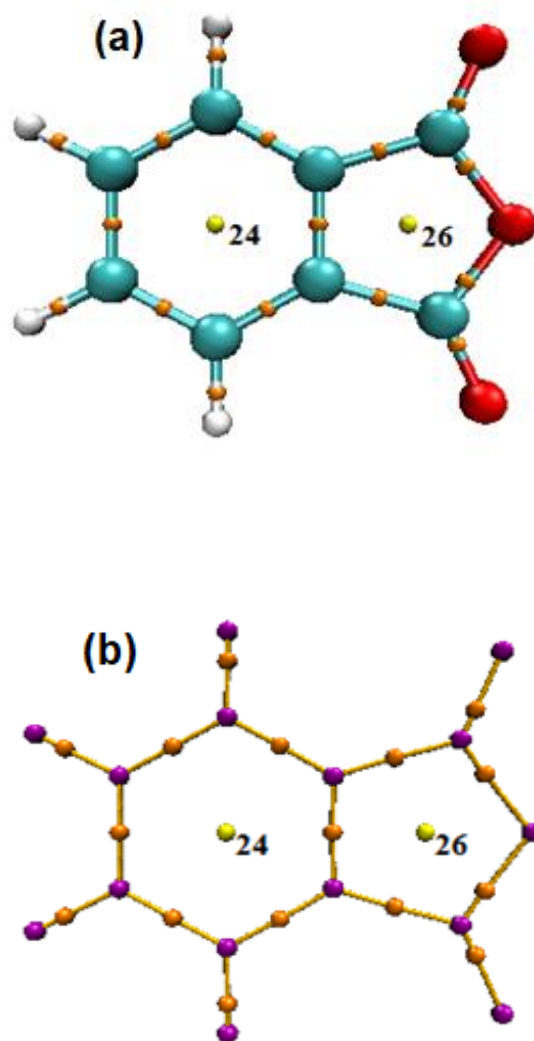


Fig. 8. (a) The resulting molecular plot displaying the critical points in the ring of compound PAN and Fig.8 (b). The molecular pattern of compound PAN in the RCPs molecular interactions seen by using the Multiwfn software.

Table 4. Ring points interaction topological parameters 24 and 26 for the molecule PAN.

Parameters (a.u)	RCP 24	RCP 26
Electron density (ρ RCP)	0.02232	0.04406
Laplacian of electron density	0.16255	0.30662
Lagrangian Kinetic Energy $G(r)$	0.03310	0.06945
Hamiltonian Kinetic Energy $K(r)$	-0.00753	-0.00721
Potential energy density $V(r)$	-0.02556	-0.06224
Eigen Value λ_1	0.09897	0.18698
Eigen Value λ_2	0.08147	0.16511
Eigen Value λ_3	-0.01788	-0.04547
Electron localization function (ELF)	0.02300	0.04910
Localized orbital locator (LOL)	0.13306	0.18518
Local information entropy	0.00238	0.00432

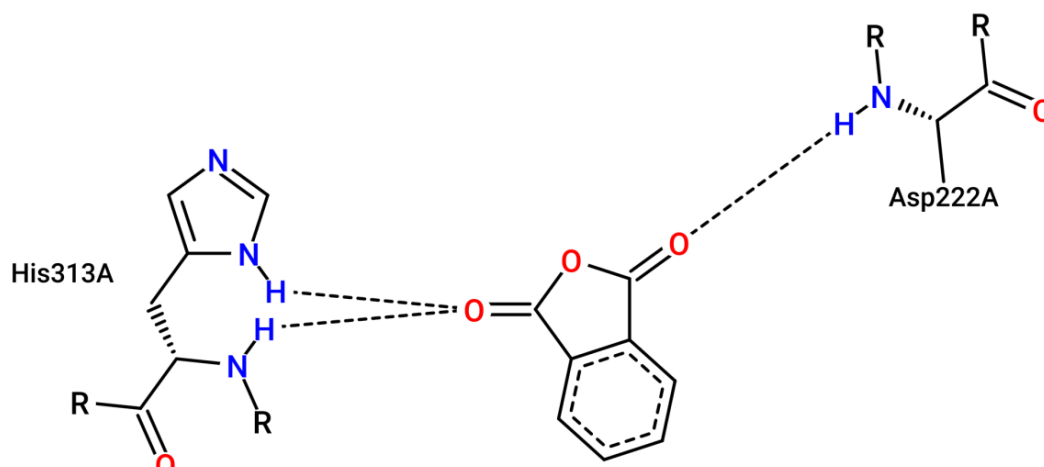


Fig. 9. Poseview diagram of PAN.

4. Conclusions

In the current study, phthalic anhydride (PAN) was effectively produced as a single crystal, and its structural and spectral properties were evaluated using examinations of single crystal X-ray diffraction, powder X-ray diffraction and FT-IR analyses. The experimental crystal structure is compared to the optimized geometric structure in the gas phase, the findings did not reveal any appreciable geometrical changes (distances and angles). The density gradient (NCL-RDG) analysis was carried out to reveal the interactions of titular compound. The geometrical and topological parameters were assessed using QTAIM analysis. The synthesised molecule has binding modes in the HIF-1 alpha fragment peptide active site, according to molecular docking experiments, and had acceptable docking scores. With the use of the internet server preADMET, the absorption, distribution, metabolism, and excretion (ADME) features were ascertained. Therefore, the titular material is nominated as a viable candidate in the field of pharmacology and medicine due to its stable structure, outstanding chemical characteristics, and strong pharmacokinetic qualities.

Acknowledgments

The corresponding author (G. Saravana Kumar) declare that they have no known competing financial interests or personal relationships that would have materialized to influence the work reported in this paper. One of the authors (N. Boukabcha) thank the Algerian Ministry of Higher Education and Scientific Research, the General Directorate of Scientific Research and Technological Development (DGRSDT) and the Hassiba Benbouali Chlef University for supporting the PRFU project number B00L01UN020120230006

Author Contributions

G. Saravana Kumar - Conceptualization, Writing – Original Draft, Supervision. M. Jeyalaxmi – Validation. N. Boukabcha - Software, Resources. K. Vijayanarasimhan - Writing – Review & Editing. A. Chouaih - Software, Resources.

References and Notes

- [1] Bray, F.; Ferlay, J.; Soerjomataram, I.; Siegel, R. L.; Torre, L. A.; Jemal, A. *CA: Canc. J. Clin.* **2018**, *68*, 394. [\[Crossref\]](#)
- [2] Kamisawa, T.; Wood, L.D.; Itoi, T.; Takaori, K. *Lancet* **2016**, *388*, 73. [\[Crossref\]](#)
- [3] Wen, Y.; Zhou, X.; Lu, M.; He, M.; Tian, Y.; Liu, L.; Wang, M.; Tan, W.; Deng, Y.; Yang, X.; Mayer, M.P.; Zou, F.; Chen, X. *Oncogene* **2019**, *38*, 1845. [\[Crossref\]](#)
- [4] Hu, L. P.; Zhang, X. X.; Jiang, S. H.; Tao, L. Y.; Li, Q.; Zhu, L. L.; Yang, M. W.; Huo, Y. M.; Jiang, Y. S.; Tian, G.A.; Cao, X. Y.; Zhang, Y. L.; Yang, Q.; Yang, X. M.; Wang, Y. H.; Li, J.; Xiao, G. G.; Sun, Y. W.; Zhang, Z. G. *Clin. Cancer Res.* **2019**, *25*, 1318. [\[Crossref\]](#)
- [5] Li, A. G.; Murphy, E. C.; Culhane, A. C.; Powell, E.; Wang, H.; Bronson, R. T.; Von, T.; Hurder, A. G.; Gelman, R. S.; Briggs, K. J.; Worms, H. P.; Zhao, J.J.; Kung, A. L.; Kaelin Jr, W. G.; Livingston, D. M. *Proc. Natl. Acad. Sci. U.S.A* **2018**, *115*, E9600. [\[Crossref\]](#)
- [6] Li, L.; Welsch, J. V.; Duffy, P. D.; Del Zoppo, G. J.; Lamanna, J. C.; Milner, R. *Glia.* **2010**, *58*, 157. [\[Crossref\]](#)
- [7] Keith, B.; Johnson, R. S.; Simon, M. C. *Nat. Rev. Cancer* **2011**, *12*, 9. [\[Crossref\]](#)
- [8] Correia, S. C.; Carvalho, C.; Cardoso, S. *Curr. Pharma. Des.* **2013**, 6809. [\[Crossref\]](#)
- [9] Aldebasi, Y. H.; Rahmani, A. H.; Khan, A. A.; Aly, S. M. *Int. J. Clin. Exp. Med.* **2013**, *6*, 239. [\[Link\]](#)
- [10] Li, Q.; Ma, R.; Zhang, M. *Oncology Letters* **2018**, *15*, 1119. [\[Crossref\]](#)
- [11] Wang, L.; Zhang, F.; Gao, X.; Luo, T.; Xu, L.; Liu, G. *Russ. J. Phys. Chem. A.* **2017**, 1432. [\[Crossref\]](#)
- [12] Fatima, A.; Khanum, G.; Sharma, A.; Garima, Km.; Savita, S.; Verma, I.; Siddiqui, N. Javed, S. *J. Mol. Str.* **2022**, 1249, 131571. [\[Crossref\]](#)
- [13] Sankar, V.; Maida Engels, S. E. *Fut. J. Pharma. Sci.* **2018**, *4*, 276. [\[Crossref\]](#)
- [14] Frisch, M. J.; Trucks, G. W.; Schlegel, H. B.; Scuseria, G. E.; Robb, M. A.; Cheeseman, J. R.; Scalmani, G.; Barone, V.; Petersson, G. A.; Nakatsuji, H.; Li, X.; Caricato, M.;

- Marenich, A.; Bloino, J.; Janesko, B. G.; Gomperts, R.; Mennucci, B.; Hratchian, H. P.; Ortiz, J. V.; Izmaylov, A. F.; Sonnenberg, J. L.; Williams-Young, D.; Ding, F.; Lipparini, F.; Egidi, F.; Goings, J.; Peng, B.; Petrone, A.; Henderson, T.; Ranasinghe, D.; Zakrzewski, V. G.; Gao, J.; Rega, N.; Zheng, G.; Liang, W.; Hada, M.; Ehara, M.; Toyota, K.; Fukuda, R.; Hasegawa, J.; Ishida, M.; Nakajima, T.; Honda, Y.; Kitao, O.; Nakai, H.; Vreven, T.; Throssell, K.; Montgomery, J. A.; Peralta, Jr., J. E.; Ogliaro, F.; Bearpark, M.; Heyd, J. J.; Brothers, E.; Kudin, K. N.; Staroverov, V. N.; Keith, T.; Kobayashi, R.; Normand, J.; Raghavachari, K.; Rendell, A.; Burant, J. C.; Iyengar, S. S.; Tomasi, J.; Cossi, M.; Millam, J. M.; Klene, M.; Adamo, C.; Cammi, R.; Ochterski, J. W.; Martin, R. L.; Morokuma, K.; Farkas, O.; Foresman, J. B.; Fox, D. J. Gaussian 09, Revision A.02, Gaussian, Inc., Wallingford CT, 2016.
- [15] Schlegel, H. B. *J. Comp. Chem.* **1982**, *3*, 214. [\[Crossref\]](#)
- [16] Hohenberg, P.; Kohn, W. *Phys. Rev.* **1964**, *136*, B864. [\[Crossref\]](#)
- [17] Becke, A. D.; *J. Chem. Phys.* **1993**, *98*, 5648. [\[Crossref\]](#)
- [18] Lee, C.; Yang, W.; Parr, R.G. *Phys. Rev. B.* **1988**, *37*, 785. [\[Crossref\]](#)
- [19] Frisch, A.; Neilson, A.B.; Holder, A.J. Gauss View User Manual, Gaussian Inc., Pittsburgh, P.A. 2000.
- [20] Bates, R. B.; Cutler, R. S. *Acta Cryst. B.* **1977**, *33*, 893. [\[Crossref\]](#)
- [21] Choudhary, V. K.; Bhatt, A. K.; Dash, D.; sharma, N. *J. Comput. Chem.* **2019**, *40*, 2354. [\[Crossref\]](#)
- [22] Foresman, J. B.; Frisch, A.; Exploring Chemistry with Electronic Structure Methods, 2nd Edition, Gaussian, Inc., Pittsburgh, P.A., 1996.
- [23] Andersson, M. P.; Uvdal, P. *J. Phys. Chem. A.* **2005**, *109*, 2937. [\[Crossref\]](#)
- [24] Stuart, B. H.; Infrared Spectroscopy: Fundamentals and Applications, John Wiley & Sons, Ltd, 2004.
- [25] Johnson, E.R.; Keinan, S.; Mori-Sanchez, P.; Contreras-García, J.; Cohen, A.J. Yang, W. *J. Am. Chem. Soc.* **2010**, *132*, 6498. [\[Crossref\]](#)
- [26] Zhang, Y.; Huang, J.; Qiao, L.; Zhang, X.; Cao, W.; Ding, Z.; Hang, X.; Qin, B.; Song, J. *J. Mol. Struct.* **2018**, *1169*, 85. [\[Crossref\]](#)
- [27] Bader, R. F. W.; Atoms in molecules – a quantum theory. Oxford University Press, Oxford, 1990.
- [28] Arulraj, R.; Roufieda, G. A.; Sivakumar, S.; Anitha, K.; Rajkumar, K.; Boukabcha, N.; Chouaih, A.; Manikandan, E. *J. Mol. Str.* **2022**, *1269*, 133845. [\[Crossref\]](#)
- [29] Lagunin, A.; Stepanchikova, A.; Filimonov, D.; Poroikov, V. *Bioinformatics* **2000**, *16*, 747. [\[Crossref\]](#)

How to cite this article

Kumar, G. S.; Jeyalaxmi, M.; Boukabcha, N.; Vijayanarasimhan, K.; Chouaih, A. *J. A. Orbital: Electron. J. Chem.* **2024**, *16*, 1. DOI: <http://dx.doi.org/10.17807/orbital.v15i5.17679>